Published in final edited form as:
Colloids Surf A Physicochem Eng Asp. 2015 January 5; 464: 134–142. doi:10.1016/j.colsurfa.2014.10.017.

Fabrication of $MnFe_2O_4$-$CuInS_2$/ZnS Magnetofluorescent Nanocomposites and Their Characterization

Violeta G. Demillo[a,b], **Mingxia Liao**[a,b], **Xiaoshan Zhu**[a,b,*], **Doug Redelman**[b,c], **Nelson G. Publicover**[a,b,d], and **Kenneth W. Hunter Jr.**[b,d]

[a]Department of Electrical and Biomedical Engineering, University of Nevada, Reno, NV, USA

[b]Biomedical Engineering Program, University of Nevada, Reno, NV, USA

[c]Department of Physiology & Cell Biology, University of Nevada, Reno, NV, USA

[d]Department of Microbiology and Immunology, University of Nevada, Reno, NV, USA

Abstract

Magnetofluorescent nanocomposites (MFNCs) providing a single nanoscale platform with multimodal properties are gaining momentum in biological manipulation, biomedical imaging and therapy. In this work, we report the preparation of MFNCs integrating $MnFe_2O_4$ magnetic nanoparticles (MNPs), $CuInS_2$/ZnS quantum dots (QDs) and poly(ethylene glycol)-b-poly(lactide-co-glycolide) (PEG-PLGA) in a tetrahydrofuran (THF)/water solvent system. Through sonication and quick solvent displacement, multiple nanoparticles of each type are co-encapsulated within the hydrophobic core of PEG-PLGA micelles. The developed fabrication process is simple and fast. Moreover, due to the low toxicity of $CuInS_2$/ZnS QDs, the fabrication process is environmentally benign. The fabricated MFNCs were further characterized regarding their fundamental physical, chemical and biological properties. Results reveal that the MFNCs possess high (Mn + Fe) recovery rates, and the optical properties and magnetic relaxivity of the MFNCs are sensitive to the MNP:QD mass ratios in the fabrication. Furthermore, the MFNCs present excellent stability in aqueous solutions, minimal cytotoxicity, and capability for bioconjugation. This study opens an avenue for the MFNCs to be employed in broad biological or biomedical applications.

INTRODUCTION

Nanocomposites integrating multiphase materials in a nanoscale domain have been paid much attention because they can be designed to gain collective or novel material characteristics from individual components. Although the fabrication of nanocomposites regarding the control of their size, shape, composition and surface properties is challenging, many recent studies have demonstrated multifunctional nanocomposites prepared from two

*To whom correspondence should be addressed : xzhu@unr.edu. Phone: 1-775-682-6298. Fax: 1-775-784-6627.

or more materials such as silica/inorganic, inorganic/inorganic, and polymer/inorganic combinations [1–6]. These nanocomposites offer synergistic physical or chemical functionalities, improved solubility in aqueous solutions, versatile surface functionalization capabilities, decreased toxicity, and/or enhanced colloidal stability when compared with each individual component. They are opening new avenues for applications in quantitative analysis, biological manipulation, biomedical imaging and therapies, energy catalysis, and more.

Development of magnetofluorescent nanocomposites (MFNCs) specially built with both magnetic nanoparticles (MNPs) and quantum dots (QDs) has been a focused topic of nanocomposite fabrication [3, 7–9]. By combining MNPs and QDs in a small domain, MFNCs not only inherit the advantages of MNPs (e.g., high saturation magnetization) and QDs (e.g., photostability, luminescence wavelength tunability), but also provide a single nanoscale platform with multimodal properties. They can enable simultaneous fluorescence labeling/imaging and magnetic field assisted separation, sorting, or heating. Moreover, when used with non-invasive magnetic resonance (MR) imaging and fluorescence imaging, MFNCs can provide dual-modality imaging that can overcome the limits of each individual imaging technology and achieve complementary merits from both imaging technologies (i.e., high spatial resolution and high sensitivity).

In this work, we mainly outline a method for fabricating MFNCs based on $MnFe_2O_4$ MNPs and $CuInS_2$/ZnS QDs and investigate their fundamental physical, chemical and biological properties. The synthesis of $MnFe_2O_4$ MNPs has been well characterized regarding particle size and shape. Furthermore these MNPs have been reported to have much stronger saturation magnetization or larger MR contrast enhancement on the T_2 weighting compared to other MNPs such as Fe_3O_4 or $CoFe_2O_4$ of the same size due to the small magnetocrystalline anisotropy and easy magnetization reversal in $MnFe_2O_4$ structure [10–14]. Core-shell $CuInS_2$/ZnS QDs are emerging materials that may serve as potential replacements for the commonly available Cd-based QDs in the biomedical and/or electronics applications due to their tunable optical properties in the visible and near infrared (NIR) region, and their low toxicity [15–20].

Regarding the fabrication of MFNCs, a number of methods have been reported. One-pot synthesis involving Cd and Fe (or Ni, Mn) precursors in organic solvents at a high temperature has been demonstrated [21–23]. In this typical approach, either magnetic atoms were doped in the CdSe lattice, or both the CdSe lattice and the magnetic Fe_2O_3 lattice can be formed in adjacent domains of MFNCs. Additionally, incorporating MNPs and Cd-based QDs into silica nano-capsules by the Stöber method has been presented [24–26]. This process is more attractive because it can produce MNFCs with biocompatible surfaces. Other options include modifying the surfaces of MNPs to have thiol groups which can further bind with Zn atoms on the shell of CdSe/ZnS QDs through ligand exchange due to the high affinity of thiols for Zn [27]. However, these methods may not be directly applicable to MFNC fabrication using $CuInS_2$/ZnS QDs. One-pot synthesis requires a balance among all precursors so that magnetic atom doping in the QD lattice can occur, or to facilitate epitaxial growth of the magnetic lattice on the QD lattice. It is challenging to find the right precursors for Cu, In, and Fe (or Ni, Mn) with the balanced reactivities to produce

MFNCs with desired properties [17, 28–30]. Moreover, involving magnetic atoms such as Mn in $CuInS_2$ core or ZnS shell may significantly change the optical properties by re-constructing the semiconductor energy band [30]. On the other hand, our lab experimental results, and some reported research by others [31], have indicated that the surface hydrophobic ligand 1-dodecanethiol (DDT) on $CuInS_2$/ZnS QDs binds very tightly with surface Zn atoms of QDs. Therefore, it is hard to be efficiently replaced by the surfactant Igepal CO-520 usually used in the Stöber method. Thus, the silica nano-capsulation method may need further revision in order to produce abundant MFNCs using $CuInS_2$/ZnS QDs. For the same reason, although the MNP surface can be modified with thiol groups for direct conjugation with Cd- based QDs, these MNPs conjugate or bind with low efficiency to DDT coated $CuInS_2$/ZnS QDs.

Amphiphilic polymer encapsulation on both MNPs and QDs to form micelles is an alternative approach for the fabrication of MFNCs [32–37]. In micellar MFNC structure, MNPs, QDs and hydrophobic chains of amphiphilic polymers form the core through hydrophobic-hydrophobic interaction, and the hydrophilic portion of the amphiphilic polymers act as the shell exposed to aqueous solutions. To fabricate micellar MFNCs, MNPs, QDs (e.g., CdSe/ZnS) and amphiphilic polymers (e.g., phospholipid-PEG copolymer) are usually dissolved in chloroform and air dried to a thin film, and then the film is hydrated in an aqueous buffer. Although this method is widely adopted for MFNC preparation, it takes a long time to air-dry chloroform [33, 35], and also involves heating for the film hydration which may be incompatible with certain functional groups on the PEG end (e.g., maleimide) [38]. Instead of the dry film method, MNPs, QDs and amphiphilic polymers also can be dissolved in tetrahydrofuran (THF), a water-miscible organic liquid with low viscosity. By adding water to this solvent system, the polarity of the solvent is progressively increased to induce the desolvation of both hydrophobic nanoparticles and hydrophobic chains of amphiphilic polymer, and thus promotes the formation of MFNCs. This approach avoids heating or hot water used in the film-hydration method. Specially, polystyrene-*block*-poly(acrylic acid) and poly-(maleic anhydride-alt-1-octadecene) were reported for the fabrication of MFNCs using Fe_2O_3 and CdSe/ZnS nanoparticles [32, 37]. However, 24-hr dialysis or magnetic separation was adopted to remove THF. Additionally, THF is not as capable as chloroform in dissolving various polymers. Cosolvents like dimethylformamide (DMF) were used to dissolve the amphiphilic polymer first. The introduction of cosolvents into the system could affect the quality of MFNCs such as fluorescence quenching. Thus, the choice of amphiphilic polymers for the THF based fabrication process is critical.

In our approach to the fabrication of MFNCs, we use PEG-PLGA (MW ~ 5000:5000 Da) amphiphilic polymer, $MnFe_2O_4$ (~ 5 nm), and $CuInS_2$/ZnS (~ 5 nm) nanoparticles dissolved in THF. As shown in Figure 1, the THF solution is layered on the top of cold water and sonicated for 1 minute using a probe-type sonicator. Under sonication, THF droplets containing PLGA- PEG, $MnFe_2O_4$ and $CuInS_2$/ZnS are formed and dispersed into water. Since THF is highly water- soluble, water displaces THF in droplets. In the process of solvent displacement, micellar MFNCs are formed. Before any further wash, THF dissolved in water is removed by 30 min rotary evaporation. Compared to reported methods, this

approach is fast in MFNC production and avoids any heating in the process due to the utilization of cold water and short-time sonication. Since PEG-PLGA is completely soluble in THF, no cosolvents are needed. Moreover, PEG chains make MFNCs more biocompatible, and they also can be easily modified to have functional head groups such as maleimide or amine or carboxyl groups for further bioconjugation. In this study, we mainly characterized the produced MFNCs in terms of their structures and size, iron content recovery rates, optical properties, magnetic relaxivity, and colloidal stability using transmission electron microscopy (TEM), dynamic light scattering (DLS), energy-dispersive x-ray spectroscopy (EDXS), UV-Vis spectroscopy, fluorescence spectroscopy, Fourier transform infrared (FT-IR) spectroscopy, magnetic resonance spectroscopy, and near infrared spectroscopy. We also performed an *in vitro* cell cytotoxicity study and a Neutravidin-biotin assay to investigate the biocompatibility and the bioconjugation capability of MFNCs, respectively.

EXPERIMENTAL METHODS

Materials and Apparatus

Copper (I) iodide (99.999%), 1-octadecene (ODE, 90%), trioctylphosphine (TOP, 90%), sulfur (99.99%), iron (III) acetylacetonate (≥ 99.9%), manganese (II) acetylacetonate, 1,2-hexadecanediol (90%), benzyl ether (98%), oleic acid (90%), and oleylamine (70%) were purchased from Sigma-Aldrich. Indium (III) acetate (99.99%), zinc stearate (ZnO 12.5–14%), 1-dodecanethiol (DDT, 98%), tetrahydrofuran (THF), hexane, ethanol and chloroform were purchased from Alfa Aesar. Methoxy poly(ethylene glycol)-*b*-poly(lactide-co-glycolide) (PEG-PLGA) (MW ~ 5000:5000 Da) and maleimide-PEG-PLGA (MW ~ 5000:5000 Da) were purchased from Akina, Inc. PEG-DSPE (MW ~ 2000:790 Dalton) was from Avanti Polar Lipids. U-87 MG and HEK-293 cells were ordered from the American Type Culture Collection (ATCC). RPMI-1640 and MEM media were from Corning Cellgro. Dulbecco's phosphate buffered saline (DPBS), phosphate buffered saline (PBS), ethylenediaminetetraacetic acid (EDTA), potassium permanganate ($KMnO_4$), potassium thiocyanate (KSCN), H_2SO_4 and $FeCl_3$ were from Fisher Scientific. Heat-inactivated fetal bovine serum (FBS) and stempro accutase were from Gibco. Fluorescein diacetate (FDA) and propidium iodide (PI) were was from Pierce. Bovine serum albumin (BSA) was from MP Biomedicals. Chemicals or reagents were used as received without further purification.

A probe-type sonicator (Misonix Ultrasonic Liquid Processor from QSonica) was used for the MFNC preparation. The ultraviolet-visible (UV-Vis) and photoluminescence spectra of QDs, MNPs, and MFNCs were obtained with a UV-Vis spectrometer (UV-2450 from Shimadzu) and spectrofluorophotometer (RF-5301PC from Shimadzu), respectively. Transmission electron microscope (TEM) images and Energy-dispersive X-ray (EDX) spectra were acquired using a JEOL analytical transmission electron microscope (model JEM 2100F operated with a 200 kV acceleration voltage) equipped with an Oxford Energy-Dispersive X-ray (EDX) spectrometer. Infrared (IR) spectra of MFNCs were collected using an FT-IR spectrometer (Perkin-Elmer Frontier) with Spectrum 10 software and the Universal ATR Sampling Accessory. The hydrodynamic sizes of MFNCs were measured using a DLS instrument (Malvern Zetasizer Nano ZS) equipped with a HeNe laser operating

at 632.8 nm and a scattering detector at 173 degrees. A Perkin Elmer microplate reader was used for the iron content assay, the MFNC colloidal stability study, and the avidin-biotin binding assay. A BD Biosciences SORP LSR II flow cytometer with 4 lasers (405 nm, 488 nm, 561 nm and 640 nm) and 18 fluorescence detectors was used to estimate cell viability and toxicity. A Bruker BioSpec 7T horizontal bore system and a Perkin Elmer IVIS system were used for magnetic resonance imaging and optical imaging of MFNCs, respectively.

Preparation of $MnFe_2O_4$ MNPs

$MnFe_2O_4$ MNPs were synthesized through a thermal decomposition method [10]. Briefly, the precursors iron(III) acetylacetonate (2 mmol), manganese acetylacetonate (1 mmol), and 1,2-hexadecanediol (10 mmol) were mixed with oleic acid (6 mmol) and oleylamine (6 mmol) in 20 mL of benzyl ether. The mixture was placed in a three-necked, round-bottom flask and degassed under vacuum for 30 min. After degassing, the mixture was heated to 200 °C for about 2 hours under argon and then heated to 290–298 °C for 30 min using a heating mantle. After cooling, ethanol was added to the mixture and the particles precipitated by centrifugation. The particles were washed using hexane and ethanol and dried under vacuum.

$CuInS_2$/ZnS QDs Preparation

$CuInS_2$/ZnS QDs were synthesized through a revised thermal decomposition method [18]. For the preparation of $CuInS_2$ nanocrystals, indium acetate (0.25 mmol), copper (I) iodide (0.25 mmol), and DDT (4.0 mL) were added into a 50 mL three-necked, round-bottom flask. The reaction solution was degassed under vacuum at room temperature until no bubbles were observed. Solutions were then heated to 140 °C under vacuum using a hot oil bath. An argon atmosphere was next introduced into the flask and the temperature of the resulting solution was raised to 240 °C. The reaction was continued until the desired CIS core emission wavelength was obtained and then the reaction flask was cooled down to room temperature and diluted with 4.0 mL ODE. To promote ZnS shell growth on CIS cores, S-precursor solution (0.4 M sulfur in DDT/TOP (4:1) at room temperature) and Zn-precursor solution (0.4 M zinc stearate in ODE at 160 °C) were injected in sequence 6 times to the diluted core growth solution at 240 °C in 1.0 mL portions at 20 minutes intervals. After reactions were complete, mixtures were cooled down to room temperature in air and $CuInS_2$/ZnS QDs were purified using hexane and ethanol, and dried under vacuum.

Fabrication of MFNCs

The solution of $MnFe_2O_4$ MNPs, $CuInS_2$/ZnS QDs, and PEG-PLGA in THF was layered on the top of cold water in a glass vial. The mixture was ultrasonicated using the Misonix Ultrasonic Liquid Processor with a 3 W output power for 1 min. After sonication, THF was removed by rotary evaporation at room temperature and the sample filtered through a 0.2 μm syringe filter to remove big aggregates. Empty micelles or single-nanoparticle based micelles were removed by centrifugation at 18,000 rpm for 25 min (twice). The collected MFNCs were then re-filtered through 0.2 μm syringe filter, concentrated using a centrifugal filter, dispersed in 600 μL of water, and stored at 4°C until further use.

Determination of (Mn + Fe) content in MFNCs

As a first step, the iron content of MFNCs was determined using thiocyanate colorimetry [39]. 100 μL of the prepared MFNCs was mixed with 5 mL of 1 M H_2SO_4 and stirred at 90 °C for 2 hours. After cooling to room temperature, the sample was transferred into a volumetric flask and potassium permanganate ($KMnO_4$, 0.2 M) was added dropwise until the purple color was retained. The flask was filled with 1 M H_2SO_4 until the solution surface reached the volume mark on the flask. Equal volumes (250 μL each) of the sample and 1M KSCN were mixed, and 100 μL of the resultant red solution was loaded into a microplate and the absorbance of the resultant solution was measured at 490 nm using the microplate reader. Solutions of $FeCl_3$ in 1 M H_2SO_4 with an iron(III) concentration range from 0 to 100 μM were used as calibration standards. These standards went through the same reaction process as the samples. If necessary, the samples were diluted to keep absorbance readings within the absorbance range of calibration standards, prior to reaction with KSCN. All glassware (and stir bar) used in the assay were pre-washed with concentrated acid to remove any iron contamination. Iron content of MFNCs was determined by interpolating the absorbance of the samples on the calibration curve. Iron content in the starting magnetic materials ($MnFe_2O_4$ MNPs) used for the MFNC preparation was also determined in the same way. After iron determination, (Mn + Fe) content in MFNCs was further determined on the basis of the atomic ratio of Mn:Fe in MNPs.

Cell Cytotoxicity of MFNCs

A U-87 MG human brain glioblastoma cell line (ATCC HTB-14) was cultured (37°C, 5% CO_2) on 48-well plastic plates in MEM medium with 10% FBS overnight. The human embryonic kidney cell line HEK-293 (ATCC CRL-1537) was cultured (37°C, 5% CO_2) on 48-well plastic plates in RPMI-1640 (Corning Cellgro) medium with 10% FBS overnight. For the MFNC cytotoxicity study, cells were incubated with MFNCs in growth medium at various concentrations. After 24-hr incubation, cells were gently rinsed with DPBS and released from well bottom using stempro accutase, and then stained with FDA/PI to determine live versus dead cells. Dead cells (red staining by PI) and live cells (green staining by FDA) were counted using a BDBiosciences SORP LSR II flow cytometer. The cell viability was calculated as the ratio of live cells over the sum of live cells and dead cells. The relative cell viability is the ratio of the cell viability of the samples to that of the control.

Conjugation of MFNCs with Neutravidin for Avidin-Biotin Binding Assay

MFNCs with the MNP:QD mass ratio at 1:4 were prepared with 75% PEG-PLGA and 25% maleimide-PEG-PLGA, and suspended in 110 μL PBS pH6.7. The thiolation of Neutravidin was completed by dispersing 2.5 nmole of Neutravidin in 100 μL of PBS (pH8, 5 mM EDTA) with 25 nmole of Traut's reagent. The prepared MFNCs were incubated with thiolated Neutravidin for 2 hours. After incubation, MFNCs were washed by centrifugation using PBS pH7.2. MFNCs without any conjugation with Neutravidin were used as controls.

Four μL of biotinylated magnetic microbeads (4.5 μm diameter, 4×10^8 beads/mL) were placed in each well of a microplate. Fifty μL of MFNC-Neutravidin conjugates in different concentrations in PBS pH7.2 were loaded into microplate wells. Unconjugated MFNCs were used as controls. The microplate was vortexed at room temperature for 30 min, and then the

magnetic microbeads in each well were washed using PBS pH7.2 with 1% BSA and dispersed in 50 μL of PBS pH7.2 with 0.1% BSA. The fluorescence signals of the suspended microbeads in wells were measured using a microplate reader at the excitation wavelength of 405 nm and the emission wavelength of 655 nm. The experiments were performed in triplicates.

RESULTS AND DISCUSSION

The $MnFe_2O_4$ and $CuInS_2$/ZnS nanoparticles were prepared based on previously reported methods [10, 18]. Compared to $MnFe_2O_4$ MNPs, $CuInS_2$/ZnS QDs present triangular shapes instead of spherical profiles. In this study, the average sizes of both particles were controlled to be around 5 nm so that both are apt to be encapsulated by PEG-PLGA. In the preparation of MFNCs, 0.6 mg of $MnFe_2O_4$ MNPs was dissolved in THF, and the masses of $CuInS_2$/ZnS QDs and PEG-PLGA in THF were adjusted to certain ratios to the mass of MNPs. The starting material conditions are listed in Table 1. It was of interest to investigate how the mass ratios of individual starting materials affect the fundamental physical/chemical characteristics of the collected MFNCs.

The size and elemental composition of micelles were characterized using TEM and EDXS. Figure 2 presents TEM images and EDX spectrum of micelles prepared with the mass ratio of $MnFe_2O_4$:$CuInS_2$/ZnS = 1:2. On the basis of TEM imaging, the representative size of MFNCs are around 30 ~ 60 nm (Figure 2(a)–(b)), and the overall size of MFNCs is mostly distributed over a range of 10 ~ 100 nm. Looking at the structure of a single MFNC, both spherical and triangular particle shapes were observed, indicating the presence of both MNP and QD, respectively. Moreover, EDX analysis (Figure 2(c)) further demonstrates that MFNCs are composed of Mn, Fe, O, Cu, In, Zn and S elements. For other mass ratios, similar MFNC sizes and morphologies were observed. The prepared MFNCs are a mixture of $MnFe_2O_4$ and $CuInS_2$/ZnS. The FT-IR spectra of materials used in producing MFNCs and the resultant MFNCs were characterized, and all FTIR spectra were shown in Figure S1 in the supplementary content. It can be seen that the peaks in the spectra of hydrophobic nanoparticles and PEG-PLGA are represented in the spectrum of MFNCs. These spectra together with the EDX data confirmed that the prepared MFNCs integrate MNP, QDs and PEG-PLGA. Specifically, the peaks at around 2921 cm^{-1} and 2852 cm^{-1} are from the CH_2 stretching vibrations present in the alkyl chains of oleic acid and dodecanethiol [40–41]. The C=O peak at 1752 cm^{-1} is due to the ester carbonyl of PLGA and the ether –CO at 1089 cm^{-1} from PEG [42]. In addition, DLS data have been collected and presented in Figure S2 of the supplementary content. The hydrodynamic sizes of MFNCs are mainly centered on 130 nm with a 65 nm standard deviation (a range of 65~ 195 nm). Although the TEM images showed a smaller size range of MFNCs, the size distribution were disclosed by both DLS and TEM measurements are not conflict with each other for the following reason. TEM imaging mainly distinguishes the sizes of micelle hydrophobic cores. In contrast, DLS measures MFNC hydrodynamic sizes mainly contributed by the micelle hydrophobic core and the PEG shell. Considering the length of 5K Dalton PEG chains (~ 30 nm), the MFNC hydrodynamic size range and the TEM measured size range are aligned well with each other.

The (Mn + Fe) content in MFNCs was quantified on the basis of the iron content determination of MFNCs using thiocyanate colorimetry [39]. The basic principle is that the iron(III) ions released from MFNCs by acid dissolution react with thiocyanate ions to form blood-red $Fe(SCN)^{2+}$complexes. The absorbance of $Fe(SCN)^{2+}$complexes was measured at 490 nm. The iron content of MFNCs was determined by interpolating the measured absorbance on a standard calibration curve. As shown in Figure S3 in the supplementary content, the thiocyanate colorimetry was found to be very specific and sensitive to iron(III), but not to other ions such as Cu(II), In(III), Zn(II), and Mn(II) which are found in MFNCs. Once iron content was determined, (Mn + Fe) content in MFNCs was then determined on the basis of the atomic ratio of Mn:Fe in MNPs. The (Mn + Fe) recovery rate of the MFNC fabrication process was further calculated as the ratio of the (Mn + Fe) content in the collected MFNCs to that in the starting magnetic materials. Table 2 shows the (Mn + Fe) recovery rate for 0.6 mg $MnFe_2O_4$ MNPs input to MFNCs. It can be seen that for the PEG-PLGA based MFNCs, the recovery rates are around 50% ~ 60% (~ 0.2 mg of the total mass of Mn and Fe) for the mass ratio of MNP:QD from 1 to 4. As a comparison, the most commonly used PEG-DSPE (MW 2000:790 Dalton) polymers in equal mole number to PEG-PLGA, were used to prepare MFNCs while keeping all other fabrication parameters unchanged. The (Mn + Fe) recovery rates for PEG-DSPE are in a wide range from 10 to 50% depending on the MNP:QD mass ratios. Moreover, the recovery rates have large standard deviations, which indicate the poor repeatability of the MFNC fabrication using equal mole number of PEG-DSPE. On the basis of experimental observations, for the use of PEG-DSPE with MNP:QD mass ratios at 1:1 and 1:2, most of MFNCs were filtered out on a 0.2 μm filter right after the rotary evaporation step, which results in low (Mn + Fe) recovery rates. Although approximately 47% recovery was achieved using PEG-DSPE with MNP:QD mass ratio at 1:4, the produced MFNCs were observed to be turbid and not as bright as the MFNCs prepared using PEG-PLGA under the same MNP:QD mass ratio. A possible explanation of these differences is that DSPE is too short in molecular structure and cannot wrap around nanoparticles as efficiently as PLGA. Therefore, relatively larger MFNCs were produced to be removed by filters or cause the final product suspension to be turbid.

The (Mn + Fe) recovery rate is an important characteristic for the MFNC fabrication process. It indicates how many fabrication batches need to be conducted in order to collect enough MFNCs for *in vivo* studies or other applications. For example, in animal imaging studies using MFNCs, ~ 10 mg/kg (Mn + Fe) per mouse body weight is required to inject into a mouse via the tail vein. For a mouse with body weight around 20 g, around ~ 0.2 mg (Mn + Fe) is needed for injection. The developed MFNC preparation approach using PEG-PLGA can produce enough (Mn + Fe) mass in this range in a single fabrication step instead of two or more steps. Moreover, the standard deviation of the recovery rate indicates whether the fabrication process is reliable. Adopting PEG-PLGA can lower fabrication cost and enhance production yield. This is a major reason why PEG-PLGA was used for MFNC fabrication in this study.

The photoluminescence (PL) of the prepared MFNCs was characterized using a spectrofluorometer. Figure 3 presents the PL spectra of MFNCs at different MNP:QD ratios. It can be seen that incorporation of more MNPs into MFNCs causes significant PL

quenching (the measured quantum yields of MFNCs are < 10 %). The quenching could be due to the effect of MNP absorption on QD emission, or caused by the blocking of MNPs on QD excitation/emission surfaces. In spite of the quenching, the overall PL property of MFNCs can be flexibly tuned by adjusting QD/MNP mass ratio in the fabrication process. It should be noted that MFNCs with low quantum yields are still adequate for optical imaging applications [43]. The absorbance of the prepared MFNCs was characterized using a UV-Vis spectrophotometer. As shown in Figure S4 in the supplementary content, no significant difference among UV-Vis absorbance curves was observed among MFNCs fabricated at different MNP:QD ratios.

The imaging features of MFNCs were further characterized using a Bruker BioSpec (MR imaging instrument) and a Perkin Elmer IVIS (optical imaging instrument). The MR image is a magnitude image of the TR/TE combination. The MR images of MFNCs were acquired with a conventional spin echo acquisition (TR = 6000 ms) with TE values ranging from 9.5 ms to 190 ms. MFNC concentration map in microplate wells and the related MR image are shown in Figure 4(a) and (b). On the basis of the MR image, the MR detection limit is in the range of 0.05 ~ 0.5 μg (Mn + Fe)/mL. T_2 parameter (or R_2 parameter, $R_2=1/T_2$) of MFNCs was further found by fitting the exponential decay of the signal waveform and measuring the signal intensity at a series of different TE values [44]. Figure S5 in the supplementary content presents R_2 parameter (or $1/T_2$) of MFNCs vs (Mn + Fe) concentration. The relaxivity (r_2) of MFNCs was calculated as the slope of each curve in Figure S3. Table 3 presents the relaxivity r_2 values of MFNCs for the different MNP:QD mass ratios. It can be seen that MNP micelles (not containing any QDs) have the highest relaxivity, and the relaxivity of MFNCs is reduced as more QDs are incorporated. Compared to the relaxivity of MNP micelles, the relaxivities of MFNCs fabricated with the mass ratios of MNP:QD at 1:1, 1:2 and 1:4 drop by around 25%, 30%, and 50%. However, their relaxivity values are still comparable to many reported ones [12, 14]. The optical properties of the MFNCs were also characterized using fluorescence imaging microscopy under appropriate excitation/emission filter settings. The fluorescence image is shown in Figure 4(c). On the basis of optical intensity in this image, 0.05 μg (Mn + Fe)/mL is detectable and the detection limit is in the range of 0 ~ 0.05μg (Mn + Fe)/mL. It is reasonable that the optical imaging has a lower detection limit because optical imaging intrinsically is more sensitive than MR imaging. Considering the MFNCs fabricated with the mass ratio of MNP:QD at 1:2 or 1:4 have higher optical brightness, they may be useful for imaging applications.

For biological or biomedical applications, it is critical that MFNCs should be colloidally stable. Aggregation or instability of MFNCs will cause the degradation or loss of their physical/chemical/biological functionalities. The PL intensity of MFNCs dispersed in PBS-5%FBS with pH 6–9 and human serum was monitored over 72 hours at 37 °C using the microplate reader. As shown in Figure 5, the photoluminescence intensity and hence stability of these MFNCs (fabricated with MNP:QD mass ratio at 1:2) was maintained in all tested solutions. The stability of MFNCs with other MNP:QD mass ratios was also tested and similar results were obtained. Additionally, the stability of all MFNCs was further monitored over one week at 37 °C. No significant PL intensity decreases were observed under these conditions. The PL intensities were re-measured after two weeks, and a ~20% PL intensity drop was found for each testing condition. These data suggest that the MFNCs

prepared under these conditions should be used within one week. Since the stability test conditions mimic the major of *in vitro* or *in vivo* experimental environments, the stability of these MFNCs offers a great deal of flexibility for their biological or biomedical applications. The MFNCs were also found to be stable in water at 4 °C over months. For long-term storage, drying the MFNCs then re-suspending them in appropriate solutions before use is another feasible approach.

To investigate the biocompatibility of MFNCs to cells or tissues, the cytotoxicity of the MFNCs was studied using human primary glioblastoma cells (U-87 MG) and human embryonic kidney 293 cells (HEK-293). U-87 MG and HEK-293 are tumor cells and normal cells, respectively. Since they may have different hardiness and resistance to the same cytotoxic environments, it was of interest to test the toxicity of MFNCs to both types of cells. Figure 6(a) and (b) shows the relative cell viabilities for U-87 MG and HEK-293 after 24-hour incubation with the MFNCs under different concentrations, respectively. It can be seen that the average cell death is no more than 10% compared to control, and the toxicity of the MFNCs is insignificant.

Finally, to demonstrate that MFNCs can be used for bioconjugation, MFNCs were fabricated with PEG-PLGA and maleimide-PEG-PLGA. These MFNCs were conjugated with thiolated Neutravidin and used in a Neutravidin-biotin binding assay. Figure 7 shows the fluorescence responses of the biotinylated magnetic microbeads after their incubation with Neutravidin conjugated MFNCs. To verify that the increased fluorescence was not due to the nonspecific binding of conjugated MFNCs on magnetic microbead surfaces, the fluorescence responses of the biotinylated magnetic microbeads after their incubation with non-conjugated MFNCs under the same concentrations were measured as controls. For each concentration, the fluorescence response for non-conjugated MFNCs is clearly lower than that of conjugated MFNCs. Thus, it is clear that MFNCs with maleimide groups can be specifically conjugated with biomolecules.

CONCLUSION

In conclusion, we have demonstrated and characterized the fabrication of MFNCs integrating $MnFe_2O_4$ MNPs and $CuInS_2$/ZnS QDs and PEG-PLGA polymers on the basis of a THF/water solvent system. The developed fabrication process is simple and fast. Through avoiding Cd-based QDs but adopt lowly toxic $CuInS_2$/ZnS QDs, the fabrication process is environmentally friendly. Moreover, considering $CuInS_2$/ZnS QDs can be tuned to emit near infrared (NIR) light in the range of 800 – 1000 nm, the MFNCs with NIR emission can be fabricated.

The fundamental physical, chemical and biological properties of the fabricated MFNCs also have been characterized, which is an important step before applying them in further applications. It is found that the MFNCs possess high (Mn + Fe) recovery rates, which further makes the fabrication cost lower and the production yield higher compared to methods using PEG-DSPE. The optical properties and magnetic relaxivity of the MFNCs can be significantly tuned by adopting the different MNP:QD mass ratios in fabrication. For any specific applications using the MFNCs, an appropriate MNP:QD mass ratio may need to

be carefully identified. In addition, the MFNCs present excellent stability in aqueous solutions including physiological media. On the basis of further cell viability study, the MFNCs have a minimal cytotoxicity. The MFNCs are also capable of bioconjugation with the incorporation of maleimide-PEG-PLGA. These unique properties of the MFNCs open an avenue for the MFNCs to serve as a multimodal platform incorporating other agents of interest such as therapeutic drugs in their hydrophobic core or targeting biomolecular probes on their hydrophilic shell for broad biological or biomedical applications.

Future work of this study will focus on the scale-up of MFNC fabrication, as well as bioimaging applications for disease diagnosis and therapy.

Supplementary Material

Refer to Web version on PubMed Central for supplementary material.

Acknowledgments

This research was supported by the National Institute of Health (NIH) through the grant #1P20GM103650-01. Cytometry operations were partially supported by the Nevada INBRE, NIH 8P20GM10344011.

References

1. Kumar SK, Krishnamoorti R. Nanocomposites: structure, phase behavior, and properties. Annu Rev Chem Biomol Eng. 2010; 1:37–58. [PubMed: 22432572]
2. Lee JE, Lee N, Kim T, Kim J, Hyeon T. Multifunctional Mesoporous Silica Nanocomposite Nanoparticles for Theranostic Applications. Acc Chem Res. 2011; 44:893–902. [PubMed: 21848274]
3. Corr SA, Akovich YPR, Gun'ko YK. Multifunctional magnetic-fluorescent nanocomposites for biomedical applications. Nanoscale Res Lett. 2008; 3:87–104.
4. Pyun J, Matyjaszewski K. Synthesis of nanocomposite organic/inorganic hybrid materials using controlled/"living" radical polymerization. Chem Mater. 2001; 13:3436–3448.
5. Dastjerdi R, Montazer M. A review on the application of inorganic nano-structured materials in the modification of textiles: focus on anti-microbial properties. Colloids Surf B. 2010; 79:5–18.
6. Sun L, Gibson RF, Gordaninejad F, Suhr J. Energy absorption capability of nanocomposites: a review. Compos Sci Technol. 2009; 69:2392–2409.
7. Quarta A, Di Corato R, Manna L, Ragusa A, Pellegrino T. Fluorescent-magnetic hybrid nanostructures: preparation, properties, and applications in biology. IEEE Trans NanoBio. 2007; 6:298– 308.
8. Mahajan KD, Fan Q, Dorcéna J, Ruan G, Winter JO. Magnetic quantum dots in biotechnology – synthesis and applications. Biotech J. 2013; 8:1424–1434.
9. Wang G, Su X. The synthesis and bio-applications of magnetic and fluorescent bifunctional composite nanoparticles. Analyst. 2011; 136:1783–1798. [PubMed: 21431200]
10. Sun S, Zeng H, Robinson DB, Raoux S, Rice PM, Wang SX, Li G. Monodisperse MFe_2O_4 (M = Fe, Co, Mn) nanoparticles. J Am Chem Soc. 2004; 126:273–279. [PubMed: 14709092]
11. Lee JH, Huh YM, Jun YW, Seo JW, Jang JT, Song HT, Kim S, Cho EJ, Yoon HG, Suh JS, Cheon J. Artificially engineered magnetic nanoparticles for ultra-sensitive molecular imaging. Nat Med. 2007; 13:95–99. [PubMed: 17187073]
12. Na HB, Song IC, Hyeon T. Inorganic nanoparticles for MRI contrast agents. Adv Mater. 2009; 21:2133–2148.
13. Lee J, Zhang S, Sun S. High-temperature solution-phase synthesis of metal-oxide nanocrystals. Chem Mater. 2013; 25:1293–1304.

14. Xu C, Sun S. New forms of superparamagnetic nanoparticles for biomedical applications. Adv Drug Deliv Rev. 2013; 65:732–743. [PubMed: 23123295]
15. Zhong H, Zhou Y, Ye M, He Y, Ye J, He C, Yang C, Li Y. Controlled synthesis and optical properties of colloidal ternary chalcogenide $CuInS_2$ nanocrystals. Chem Mater. 2008; 20:6434–6443.
16. Li L, Daou T, Texier I, Chi T, Liem N, Reiss P. Highly luminescent $CuInS_2$/ZnS core/shell nanocrystals: cadmium-free quantum dots for in vivo imaging. Chem Mater. 2009; 21:2422–2429.
17. Xie R, Rutherford M, Peng X. Formation of high-quality I III VI semiconductor nanocrystals by tuning relative reactivity of cationic precursors. J Am Chem Soc. 2009; 131:5691–5697. [PubMed: 19331353]
18. Li L, Pandey A, Werder DJ, Khanal BP, Pietryga JM, Klimov VI. Efficient synthesis of highly luminescent copper indium sulfide-based core/shell nanocrystals with surprisingly long-lived emission. J Am Chem Soc. 2011; 133:1176–1179. [PubMed: 21207995]
19. Zhong H, Bai Z, Zou B. Tuning the luminescence properties of colloidal I–III–VI semiconductor nanocrystals for optoelectronics and biotechnology applications. J Phys Chem Lett. 2012; 3:3167–3175.
20. Deng D, Chen Y, Cao J, Tian J, Qian Z, Achilefu S, Gu Y. High-quality CuInS2/ZnS quantum dots for in vitro and in vivo bioimaging. Chem Mater. 2012; 24:3029–3037.
21. Selvan ST, Patra PK, Ang CY, Ying JY. Synthesis of silica-coated semiconductor and magnetic quantum dots and their use in the imaging of live cells. Angew Chem. 2007; 119:2500–2504.
22. Ang CY, Giam L, Chan ZM, Lin AWH, Gu H, Devlin E, Papaefthymiou GC, Selvan ST, Ying JY. 2009 Facile synthesis of Fe2O3 nanocrystals without Fe(CO)5 precursor and one-pot synthesis of highly fluorescent Fe2O3-CdSe nanocomposites. Adv Mater. 2009; 21:869–873.
23. Singh N, Charan S, Sanjiv K, Huang SH, Hsiao YC, Kuo CW, Chien FC, Lee TC, Chen P. Synthesis of tunable and multifunctional Ni-doped near-infrared QDs for cancer cell targeting and cellular sorting. Bioconjugate Chem. 2012; 23:421–430.
24. Lee J, Lee Y, Youn JK, Na HB, Yu T, Kim H, Lee SM, Koo YM, Kwak JH, Park HG, Chang HN, Hwang M, Park JG, Kim J, Hyeon T. Simple synthesis of functionalized superparamagnetic magnetite/silica core/shell nanoparticles and their application as magnetically separable high-performance biocatalysts. Small. 2008; 4:143–152. [PubMed: 18189246]
25. Ding HL, Zhang YX, Wang S, Xu JM, Xu SC, Li GH. Fe_3O_4@SiO_2 core/shell nanoparticles: The silica coating regulations with a single core for different core sized and shell thickness. Chem Mater. 2012; 24:4572–4580.
26. Fang C, Bhattarai N, Sun C, Zhang M. Functionalized nanoparticles with long-term stability in biological media. Small. 2009; 5:1637–1641. [PubMed: 19334014]
27. Wang D, He J, Rosenzweig N, Rosenweig Z. 2004 Superparamagnetic Fe_2O_3 beads-CdSe/ZnS quantum dots core-shell nanocomposite particles for cell separation. Nano Lett. 2004; 4:409–413.
28. Buonsanti R, Milliron DJ. Chemistry of Doped Colloidal Nanocrystals. Chem Mater. 2013; 25:1305–1317.
29. Jana S, Srivastava BB, Jana S, Bose R, Pradhan N. Multifunctional doped semiconductor nanocrystals. J Phy Chem Lett. 2012; 3:2535–2540.
30. Manna G, Jana S, Bose R, Pradhan N. Mn-doped Multinary CIZS and AIZS nanocrystals. J Phy Chem Lett. 2012; 3:2528–2534.
31. Foda MF, Huang L, Shao F, Han HY. Biocompatible and highly luminescent near-infrared CuInS2/ZnS quantum dots embedded silica beads for cancer cell imaging. ACS Appl Mater Interfaces. 2014; 6:2011–2017. [PubMed: 24433116]
32. Kim BS, Taton TA. Multicomponent nanoparticles via self-assembly with cross-linked block copolymer surfactants. Langmuir. 2007; 23:2198–2202. [PubMed: 17279714]
33. Park JH, von Maltzahn G, Ruoslahti E, Bhatia SN, Sailor MJ. Micellar hybrid nanoparticles for simultaneous magnetofluorescent imaging and drug delivery. Angew Chem. 2008; 120:7394–7398.
34. Kim J, Lee JE, Lee SH, Yu JH, Lee JH, Park TG, Hyeon T. Designed fabrication of a multifunctional polymer nanomedical platform for simultaneous cancer-targeted imaging and magnetically guided drug delivery. Adv Mater. 2008; 20:478–483.

35. Erogbogbo EF, Yong KT, Hu R, Law WC, Ding H, Chang CW, Prasad PN, Swihart MT. Biocompatible magnetofluoresent probes: luminescent silicon quantum dots coupled with superparamagnetic iron(III) oxide. ACS Nano. 2010; 4:5131–5138. [PubMed: 20738120]
36. Kim HM, Lee H, Hong KS, Cho MY, Sung MH, Poo H, Lim YT. Synthesis and high performance of magnetofluorescent polyelectrolyte nanocomposites as MR/near-infrared multimodal cellular imaging nanoprobes. ACS Nano. 2011; 5:8230–8240. [PubMed: 21932788]
37. Di Corato R, Bigall NC, Ragusa A, Dorfs D, Genovese A, Marotta R, Manna L, Pellegrino T. Multifunctional nanobeads based on quantum dots and magnetic nanoparticles: Synthesis and cancer cell targeting and sorting. ACS Nano. 2011; 5:1109–1121. [PubMed: 21218823]
38. Tong S, Hou S, Ren B, Zheng Z, Bao G. Self-assembly of phospholipid-PEG coating on nanoparticles through dual solvent exchange. ACS Nano. 2011; 11:3720–3726.
39. Woods J, Mellon M. Thiocyanate method for iron: a spectrophotometric study. Ind Eng Chem Anal Ed. 1941; 13:551–554.
40. Mahdavi M, Ahmad MB, Haron M, Namvar F, Nadi B, Rahman M, Amin J. Synthesis, surface modification and characterization of biocompatible magnetic iron oxide Nanoparticles for biomedical applications. Molecules. 2013; 18:7533–7548. [PubMed: 23807578]
41. Chang J, Waclawik ER. Controlled synthesis of $CuInS_2$, Cu_2SnS_3 and Cu_2ZnSnS_4 nano-structures: insight into the universal phase-selectivity mechanism. Cryst Eng Comm. 2013; 15:5612–5619.
42. Yousefi G, Tamaddon A, Parhizgar E. Synthesis of PEG-PLGA copolymer for preparation of docetaxel nanoparticles. Res Pharm Sci. 2012; 7:S272.
43. Zimmer J, Kim S, Ohnishi S, Tanaka E, Frangioni J, Bawendi M. Size series of small indium arsenide-zinc selenide core-shell nanocrystals and their application in in vivo imaging. J Am Chem Soc. 2006; 128:2526–2527. [PubMed: 16492023]
44. Laurent S, Forge D, Port M, Roch A, Robic C, Elst LV, Muller RN. Magnetic iron oxide nanoparticles: synthesis, stabilization, vectorization, physicochemical characterizations, and biological Applications. Chem Rev. 2008; 108:2064–2110. [PubMed: 18543879]

Highlights

- The MFNCs integrating $MnFe_2O_4$ MNPs, $CuInS_2$/ZnS QDs and PEG5k-PLGA5k were prepared.
- The MFNC fabrication process is simple and possesses high (Mn + Fe) recovery rates.
- The MFNC optical and magnetic properties are sensitive to the MNP:QD mass ratio.
- The MFNCs have colloidal stability, low toxicity, and bioconjugation capability.
- The MFNCs may have broad biological and biomedical applications.

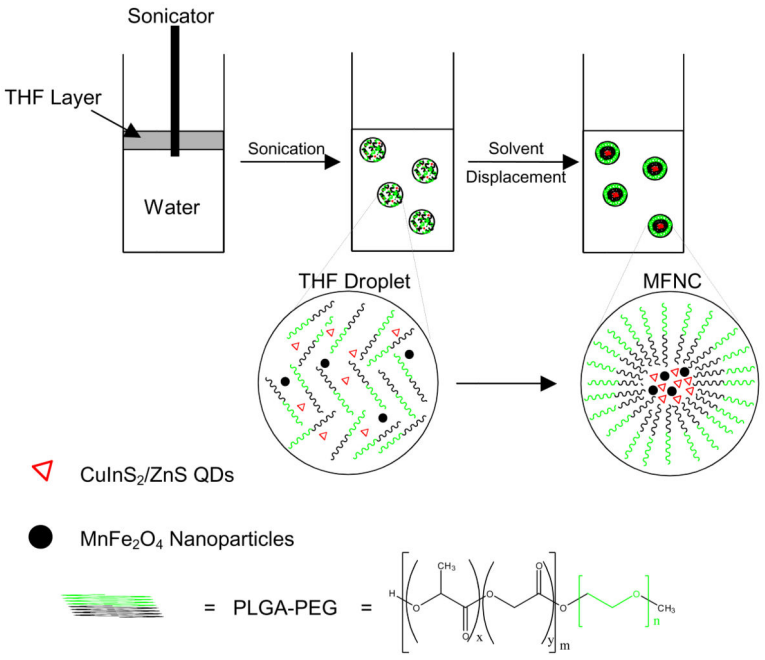

Figure 1.

Scheme of the MFNC fabrication process using PEG-PLGA, $MnFe_2O_4$ MNPs and $CuInS_2$/ZnS QDs in a THF/water solvent system with sonication – After sonication, THF droplets containing particles and polymers are formed and dispersed in water; highly water-soluble THF in droplets is displaced by water, which induces the self-assembling of PEG-PLGA to form micellar MFNCs co-encapsulating both MNPs and QDs.

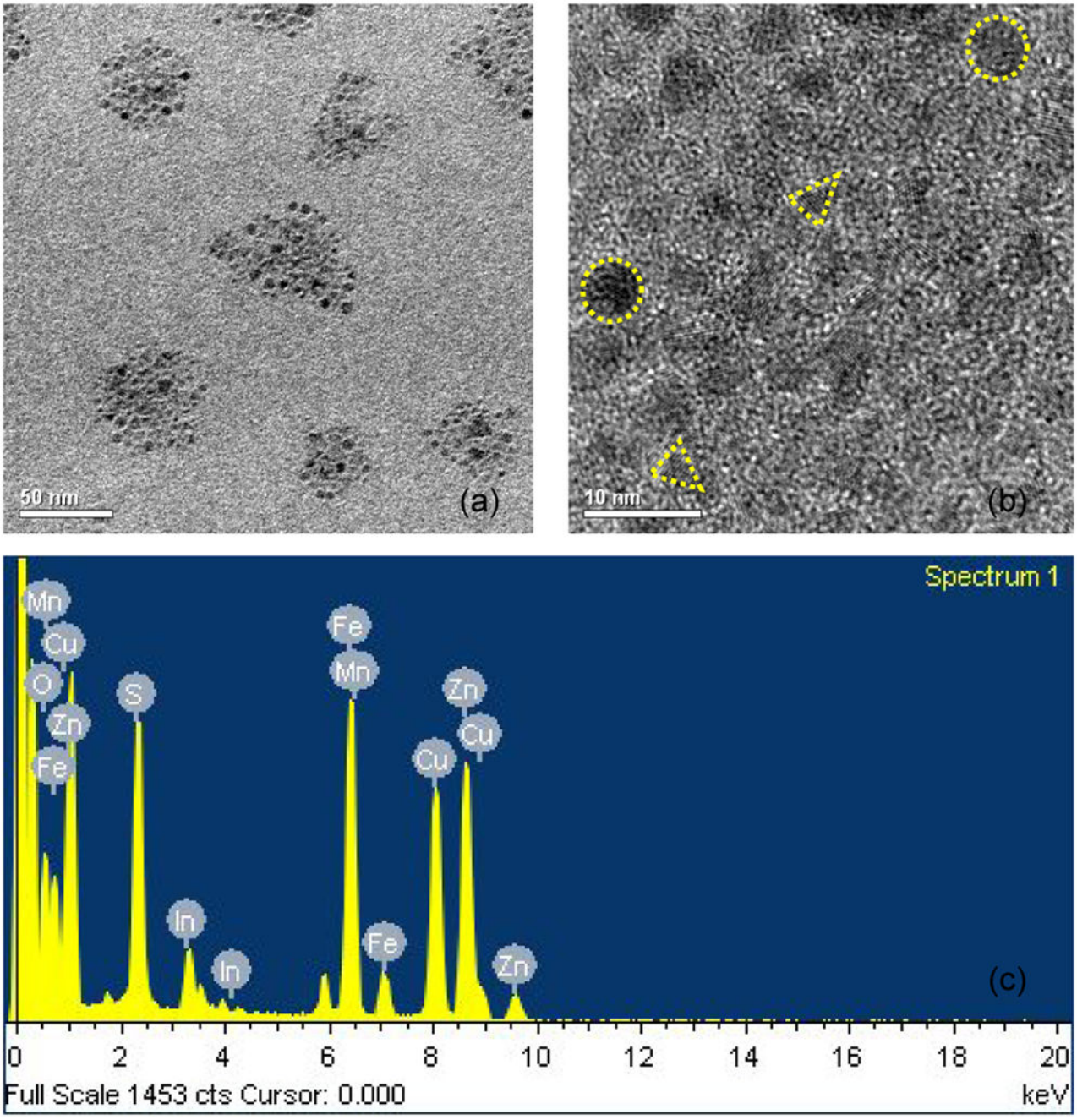

Figure 2.

(a) TEM images of MFNCs with an MNP:QD mass ratio of 1:2; (b) Magnified TEM image of a single MFNC with crystal lattices of MNPs and QDs (spherical MNPs and triangle QDs); and (c) EDX spectrum of MFNCs which illustrates Mn, Fe, O, Cu, In, Zn and S elements which are composites of MNPs and QDs.

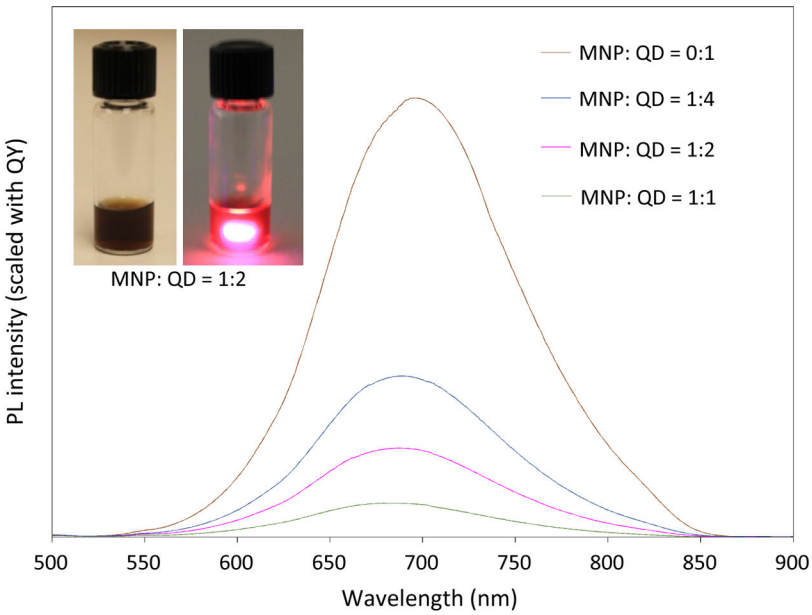

Figure 3.

PL spectra of water-soluble QD micelles (not containing MNPs) and MFNCs (Inset: the photos of MFNCs fabricated with MNP: QD = 1:2 under natural light and UV light, respectively)

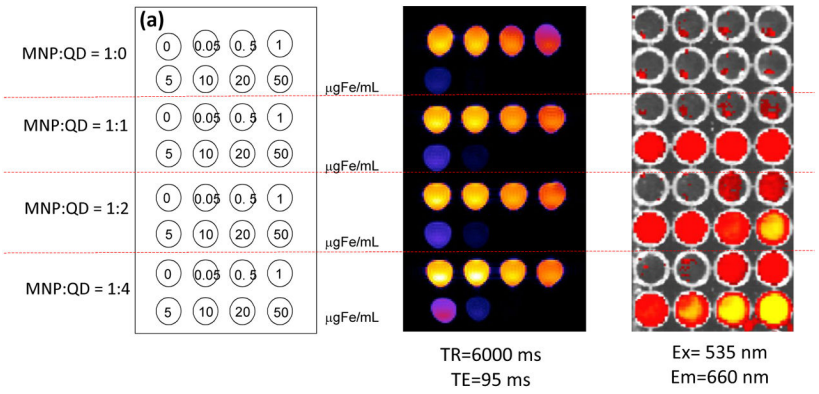

Figure 4.

(a) MFNC concentration map in microplate wells; and (b) and (c) Representative MR image and optical image of MFNCs fabricated with the MNP:QD mass ratios at 1:0, 1:1, 1:2, and 1:4. MNP micelles were fabricated as a reference for both MR and optical imaging measurement.

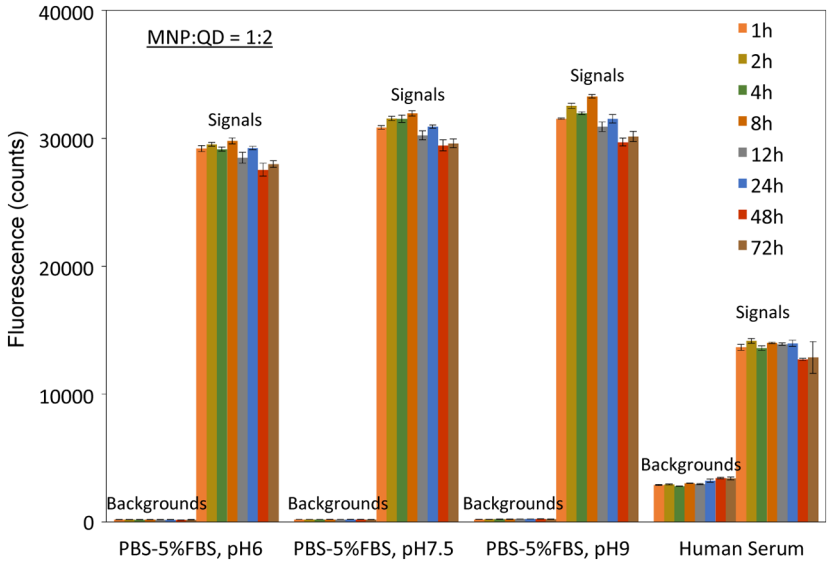

Figure 5.

Fluorescence stability of MFNCs in PBS-5%FBS with different pHs over hours at 37 °C – The MFNCs were prepared with MNP:QD = 1:2, and the fluorescence stability indicates the colloidal stability of MFNCs in the aqueous solutions (human serum is slightly turbid which causes MFNC fluorescence signals for human serum are relatively low)

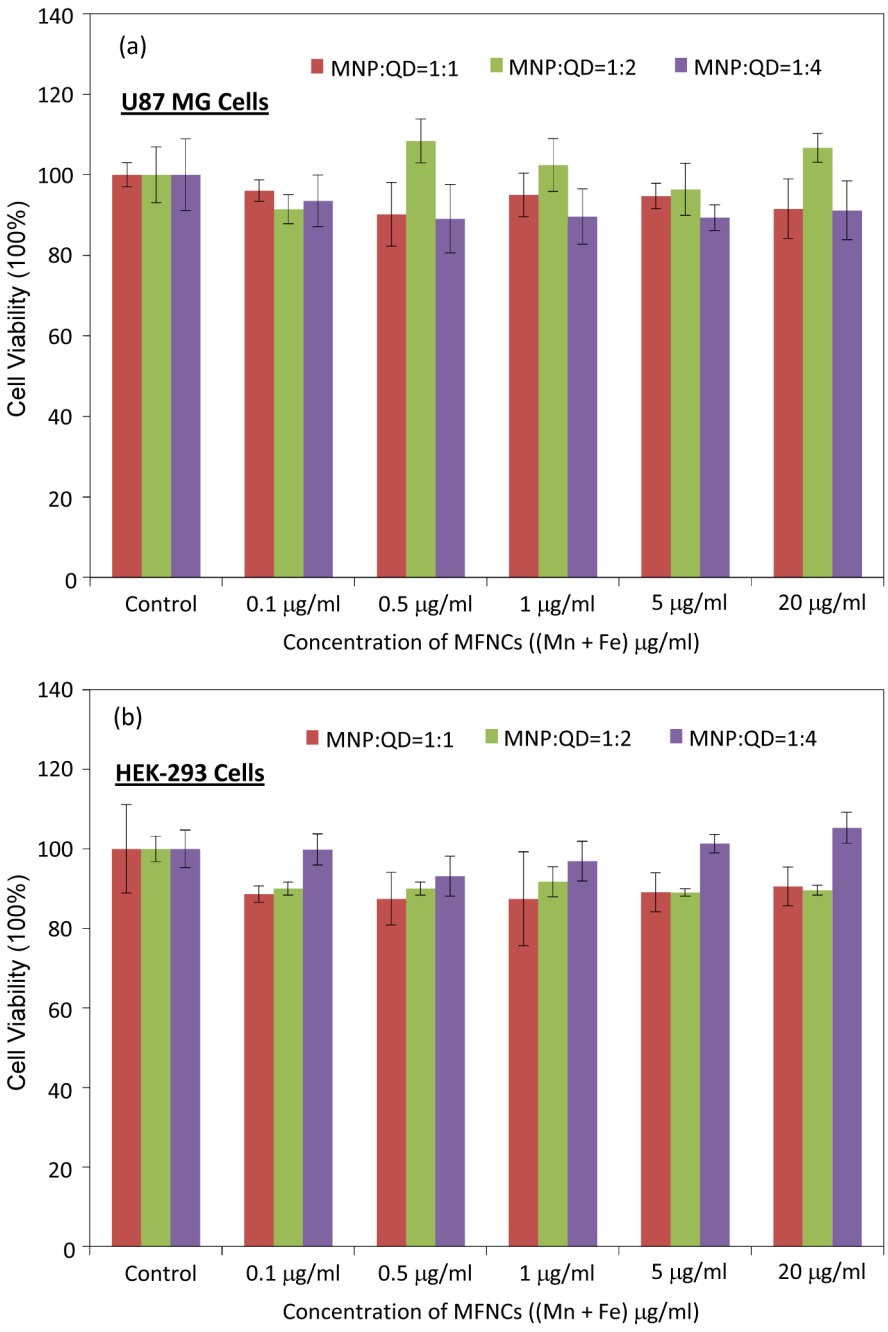

Figure 6.

Relative cell viability of U-87 MG cell (a) and HEK-293 cells (b) treated with MFNCs at difference concentrations over 24 hours – Both the MFNC concentrations and the MNP:QD mass ratios for the MFNC fabrication have no significant effects on cell cytotoxicity.

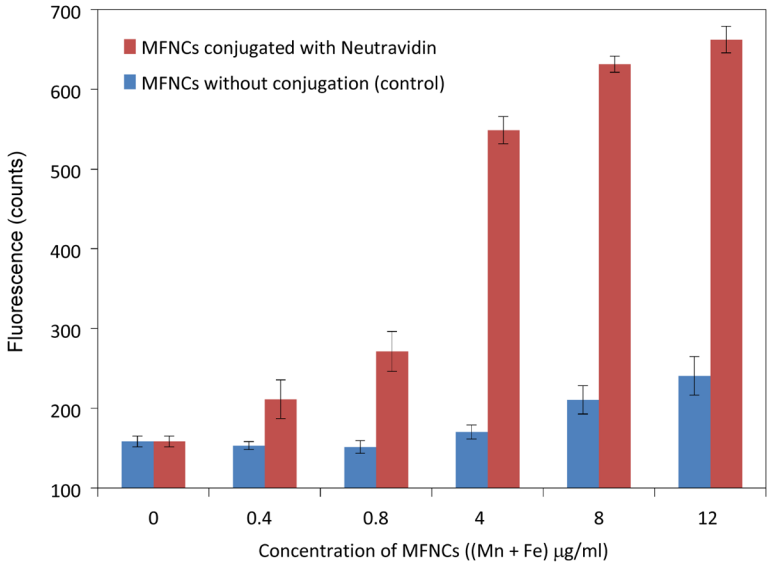

Figure 7.

Fluorescent responses of biotinylated magnetic microbeads after their incubation with non-conjugated MFNCs (blue bars) and Neutravidin-conjugated MFNCs (red bars)

Table 1

The starting material mass conditions for MFNC preparation

Mass Ratio	$MnFe_2O_4$ MNPs (mg)	$CuInS_2$/ZnS QDs (mg)	Total PEG-PLGA (mg)
MNP: QD = 1:0	0.6	0	4.8
MNP: QD = 1:1	0.6	0.6	7.2
MNP: QD = 1:2	0.6	1.2	9.6
MNP: QD = 1:4	0.6	2.4	14.4

Table 2

(Mn + Fe) recovery rates (%) in the MFNC preparation

Mass Ratio	PEG-PLGA Based MFNCs	PEG-DSPE Based MFNCs
MNP: QD = 1:1	56.28 ± 4.85	11.32 ± 11.61
MNP: QD = 1:2	53.55 ± 2.23	15.20 ± 14.37
MNP: QD = 1:4	63.31 ± 4.40	47.68 ± 10.93

Table 3

Relaxivity r_2 values of the MFNCs and MNP micelles in the T_2-weighted MR images

Mass Ratio	MNP:QD = 1:0	MNP:QD = 1:1	MNP:QD = 1:2	MNP:QD = 1:4
Relaxivity r_2 ({(Mn + Fe) mM }$^{-1}$ s^{-1})	239.6	183.3	165.4	130.9